STRUCTURAL SCIENCE
CRYSTAL ENGINEERING
MATERIALS

Volume 74 (2018)

Supporting information for article:

Triamterene–furosemide salt: structural aspects and physicochemical evaluation

Bo Peng, Jian-Rong Wang and Xuefeng Mei

Materials and Methods

Materials. Triamterene (**Tri**) and furosemide (**Fur**) with purity greater than 98.0% were obtained from Adamas Reagent (Shanghai, China) Co., Ltd. All analytical-grade solvents were purchased from Sinopharm Chemical Reagent Co., Ltd without further purification.

Preparation of Triamterene-Furosemide (Tri-Fur). Tri-Fur powder was prepared using the solution condensing method. Equal moles of **Tri** (126.63 mg, 0.5 mmol) and **Fur** (165.37 mg, 0.5 mmol) were dissolved in 16 mL of Tetrahydrofuran (THF), Acetone, and H_2O (1:1:1, V/V/V). Then, the solution was condensed at 70 °C in a glass vial. Plate shape salt of **Tri-Fur** suited for single crystal structure determination was obtained successfully. Bulk powder sample were produced by grinding the **Tri-Fur** single crystal.

Single Crystal X-ray Diffraction (SCXRD). Single crystal X-ray diffraction of **Tri-Fur** was performed at 220 K on a Bruker Apex II CCD diffractometer using Mo-Kα radiation (0.71073 Å). Data integration and scaling of intensity was performed using the SAINT program. The multiscan absorption corrections were used by the SADABS. The structure was solved by direct methods and refined with full-matrix least-squares technique using SHELX-2014 program. Non-hydrogen atoms were refined with anisotropic displacement parameters of 1.50 times U_{eq} of the parent atoms, the hydrogen atoms were placed in calculated positions and refined with a riding model. The data with .cif format have been deposited in the Cambridge Crystallographic Data Center, CCDC No. 1850982 for **Tri-Fur**. Crystallographic data and detailed refinement information are listed in Table S1.

Powder X-ray Diffraction (PXRD). PXRD patterns were collected using a Bruker D8 Advance X-ray diffractometer system with Cu-Kα radiation (1.54059 Å). The tube voltage and current were set to 40 kV and 40 mA, respectively. The sample was measured by a scan at the scan rate of 5 °/min with 2θ ranged from 3 to 40°. The data were imaged and integrated with RINT Rapid. The peaks were analyzed with Jade 6.0 from Rigaku.

Thermogravimetric Analysis (TGA). Thermogravimetric analysis was performed using the Netzsch TG 209F3 analyzer. Samples were placed in aluminum oxide pans and heated from 10 °C to 400 °C at the heating rate of 10 °C/min under the dry nitrogen flow rate of 20 mL/min purge.

Differential Scanning Calorimetry (DSC). DSC of all the samples was conducted on a DSC Q2000 (TA) instrument. The 2-3 mg ground samples were placed in sealed non-hermetic aluminum pans and heated at a heating rate of 10 °C/min from 40 to 350 °C under nitrogen gas flow of 50 mL/min purge. Two-point calibration using indium and tin was carried out to check the temperature axis and heat flow of the equipment.

Dynamic Vapor Sorption (DVS). The water sorption and desorption processes were carried out on an Intrinsic DVS instrument from Surface Measurement Systems, Ltd. The samples were mounted on a balance and studied over a humidity range from 0 to 95% RH, and then decreased to 0% RH at 25 °C. Each humidity step was made if less than a 0.02% weight change occurred over 10 min.

Polarized Light Microscopy (PLM). The PLM photo for **Tri-Fur** salt was obtained using a XPV-400E polarizing microscope and a JVC TK-C9201 EC digital video recorder (Shanghai Changfang Optical instrument Company Ltd). Selective PLM photo magnified 50 times was presented in Fig. S2.

Confocal Raman Spectroscopy. Raman spectra were measured with the Thermo Scientific DXR Raman microscope equipped with a 780 nm laser in the range from 400 to 3300 cm^{-1}. Samples were analyzed in a glass len directly by using 100 mW laser power, 50 μm slit spectrograph aperture. The 2 s exposure time and 32 sample exposures were performed for each spectrum measured.

Solubility Experiments. Equilibrium solubility was measured by suspending the **Fur**, physical mixture (PM) of **Fur** and **Tri** at molar ratio of 1:1, and **Tri-Fur** salt with excess amount in 1.0 mL of glycine-hydrochloric acid buffer (pH = 2.0) at 25 °C for 24 h, respectively. The concentrations of the solutions after centrifuging at the 14000 rpm and being filtered by passing through a 0.45 μm syring filters were measured using high performance liquid chromatography (HPLC).

IDR Experiments. IDR measurements were carried out using a Mini-Bath dissolution device equipped with a Julabo ED-5 heater/circulator. 4 mg of **Fur** and **Tri-Fur** salt were compressed into a 0.07 cm^2 disk and then were added to dissolution vessels containing 5 mL of glycine-hydrochloric acid buffer (pH = 2.0). The 100 μL sample was collected in IDR experiments. The IDR experiments were performed at 37 °C with the rotation speed of 100

rpm. The samples were performed at 5, 10, 20, 30, 60, 80 min. All the measurements were repeated three times and the average value were analyzed.

HPLC Analysis of Fur. Agilent 1260 series HPLC (Agilent Technologies) equipped with a ZORBAX Eclipse Plus C18 analytical column (4.6 mm × 150 mm, 5 μm) and a quaternary pump G1311C was used to analyze the concentration of **Fur**. The 1260 variable wavelength detector G7114A (VWD) was set at 233 nm. The mobile phase consisting of acetonitrile and 10 mM KH_2PO_4 buffer (pH = 2.6) was used at a flow rate of 1.0 mL/min with the 25 °C column temperature. The mobile phase of 10 mM KH_2PO_4 buffer used was filtered by passing through a 0.45 μm pore size membrane filter prior to use. To determine the **Fur** content, a gradient system was employed and listed in Table S3. The HPLC chromatogram of **Fur** was shown in Fig. S11.

HPLC Analysis of Tri. Agilent 1260 series HPLC (Agilent Technologies) equipped with a ZORBAX Eclipse Plus C8 analytical column (4.6 mm × 150 mm, 5 μm), a quaternary pump G1311C, and the 358 nm variable wavelength detector G7114 (VWD) were used to analyze the concentration of **Tri**. The methanol and pH 3.8 0.05 M KH_2PO_4 buffer were used at 1.0 mL/min flow rate. The column temperature was 30 °C. Firstly, the gradient system started at 70% 0.05 M $K_4H_2PO_4$ and 30% MeOH, which were maintained for 6 minutes. Secondly, the gradient system composed of 40% 0.05 M KH_2PO_4 and 60% MeOH were used to maintain for 2 minutes. Thirdly, the gradient system composed of 70% 0.05 M $K_4H_2PO_4$ and 30% MeOH were used to maintain for 2 minutes.

Table S1 Crystallographic Data for **Tri-Fur**.

Crystal data	**Tri-Fur**
Chemical Formula	$C_{24}H_{22}ClN_9O_5S$
Crystal system	triclinic
Space group	*P*-1
Temperature (*K*)	220
a (Å)	7.522 (5)

b (Å)	8.110 (5)
c (Å)	20.892 (14)
α (°)	92.574 (16)
β (°)	98.836 (17)
γ (°)	103.844 (16)
V (Å^3)	1218.2 (14)
D_{Cal}(g/cm^3)	1.592
Z	2
λ	0.71073 (Mo-Kα)
Independent reflns.	5463
S	0.975
R_{int}	0.0588
R_1	0.0571
wR_2	0.1326

Table S2 The geometrical parameters describing the intermolecular and intramolecular hydrogen bonds for **Tri-Fur**.

Crystal form	Interactions	H…A (Å)	D…A (Å)	<D-H…A (º)	Symmetry code
Tri-Fur	N1-H1…O3 (Inter)	1.95	2.810 (4)	168	x, y, z
	N2-H2A…O4 (Inter)	2.10	2.939 (5)	160	1+x,1+y,z

N2-H2B…O1 (Inter)	1.87	2.663 (4)	150	x, y, z
N4-H4A…N3 (Inter)	2.10	2.971 (5)	175	2-x,2-y,1-z
N4-H4B…N5 (Intra)	2.43	2.750 (5)	102	x, y, z
N4-H4B…O4 (Inter)	2.28	2.961 (4)	135	1-x,1-y,1-z
N7-H7A…N6 (Inter)	2.19	3.052 (5)	173	-x,1-y,1-z
N7-H7B…O3 (Inter)	2.24	2.876 (4)	130	-x,1-y,1-z
N8-H8…O1 (Intra)	1.97	2.611 (4)	130	x, y, z
N9-H9A…Cl1 (Intra)	2.63 (4)	3.277 (4)	129 (3)	x, y, z
N9-H9B…O1 (Inter)	2.04 (4)	2.815 (5)	165 (4)	x,-1+y,z
C2-H2…N7 (Intra)	2.60	3.064 (5)	111	x, y, z
C15-H15A…O5 (Inter)	2.49	3.239 (5)	133	1+x,1+y,z
C18-H18…O3 (Intra)	2.41	2.752 (5)	101	x, y, z
C18-H18…O4 (Intra)	2.46	2.856 (4)	106	x, y, z

Table S3 Gradient HPLC system for the determination of **Fur** content.

Time (min)	10 mM KH_2PO_4 %	ACN %	Flow rate (mL/min)
0	70	30	1.0
2	60	40	1.0
8	60	40	1.0
8.01	70	30	1.0
10	70	30	1.0

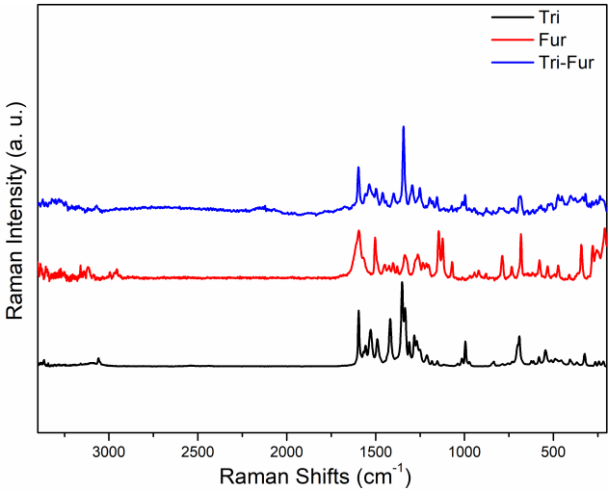

Figure S1 The Raman spectra of **Tri**, **Fur** and **Tri-Fur**.

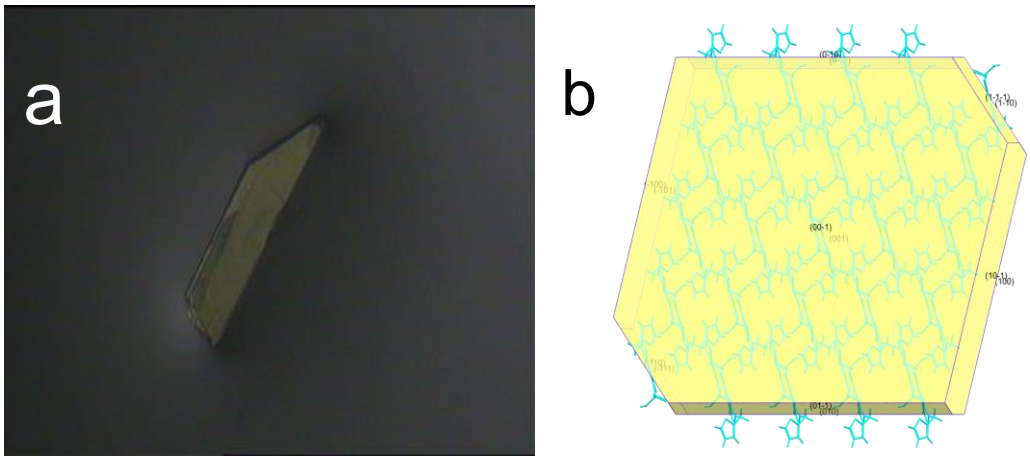

Figure S2 Polarized light microscopy (magnified 50 times) (a) and Bravais, Friedel, Donnay and Harker (BFDH) prediction (b) of **Tri-Fur**.

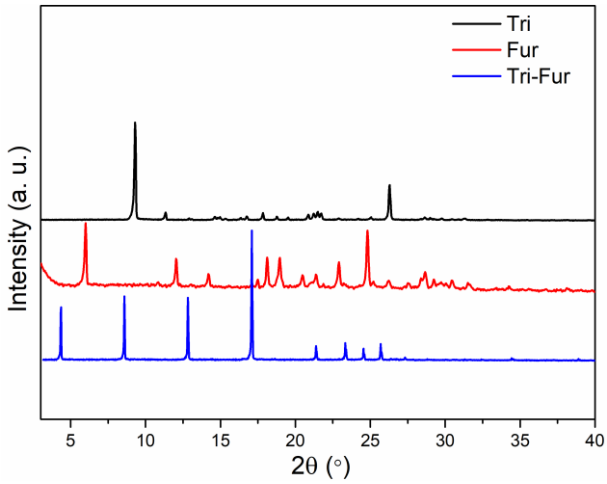

Figure S3 The experimental PXPD of **Tri**, **Fur** and **Tri-Fur**.

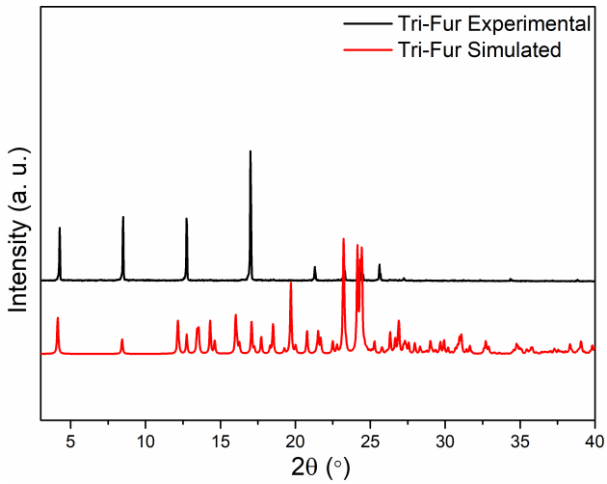

Figure S4 Comparison between experimental and simulated PXPD of **Tri-Fur**.

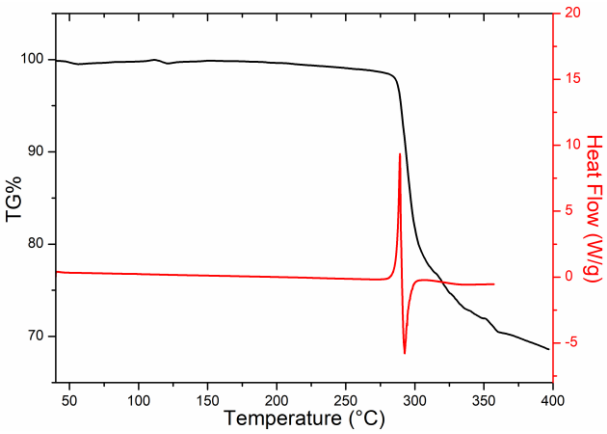

Figure S5 TG and DSC curve of **Tri-Fur**.

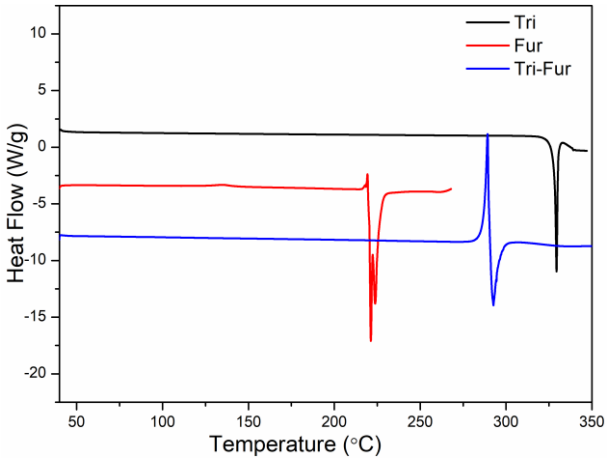

Figure S6 Comparison of DSC curve among **Tri**, **Fur** and **Tri-Fur**.

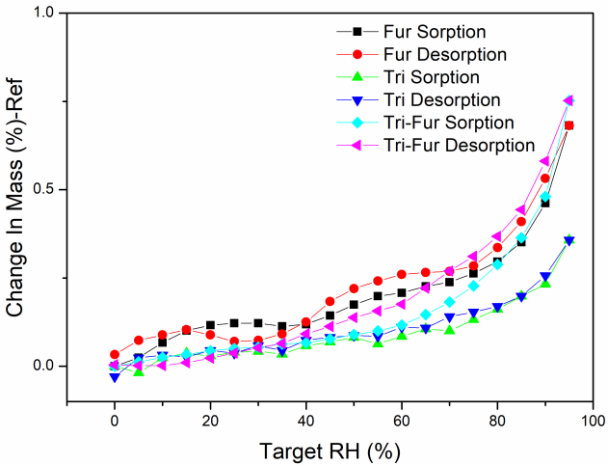

Figure S7 Water vapour sorption and desorption isotherm curves of **Tri**, **Fur**, and **Tri-Fur**.

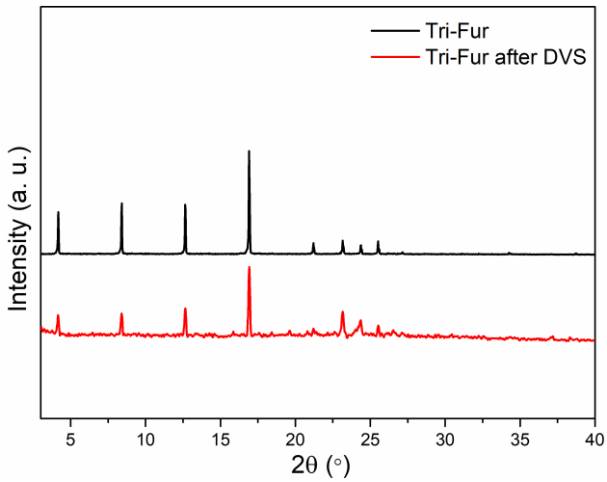

Figure S8 XRPD patterns of **Tri-Fur** before and after DVS experiments.

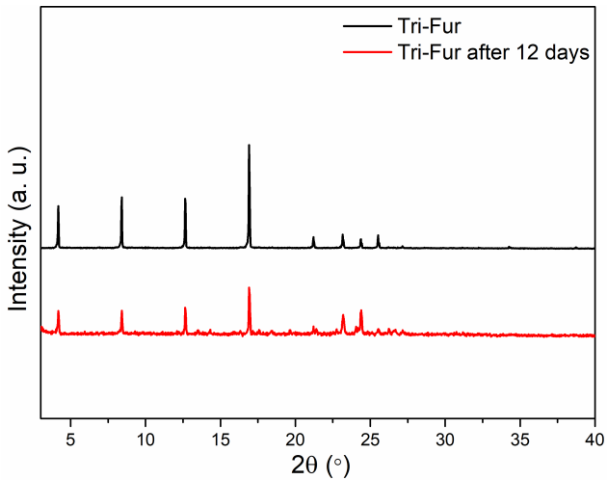

Figure S9 XRPD patterns of **Tri-Fur** before and after accelerated stability test.

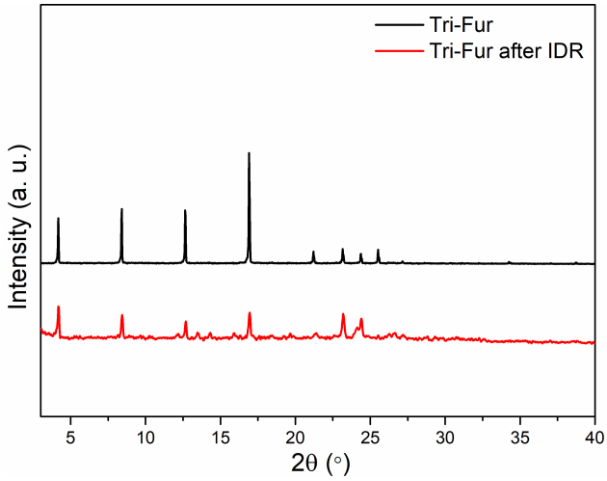

Figure S10 XRPD patterns of **Tri-Fur** salt before and after IDR test.

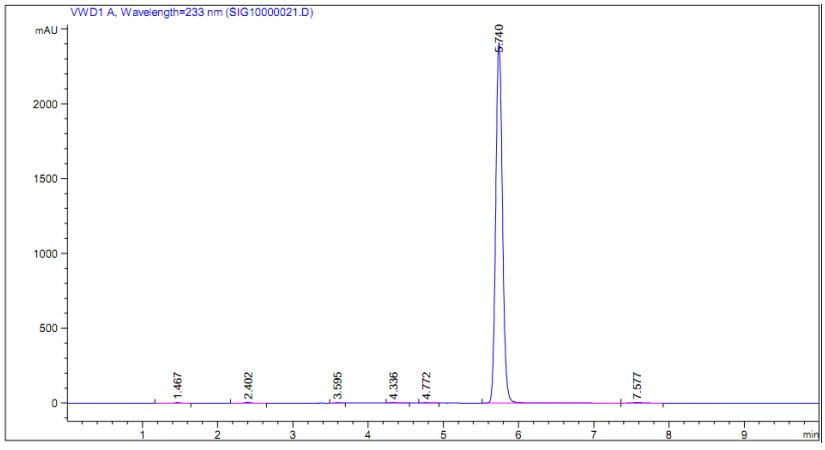

Figure S11HPLC chromatogram of **Fur**.

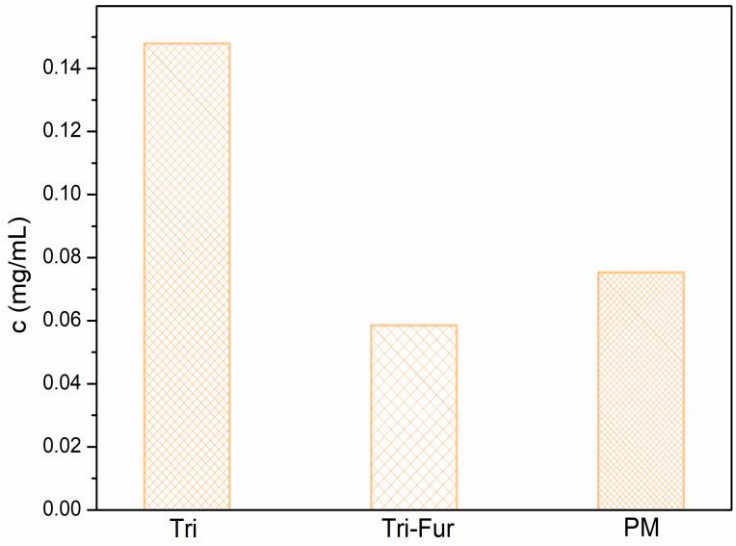

Figure S12 Apparent equilibrium solubility of **Tri**, PM of **Tri** with equimolar **Fur**, and **Tri-Fur** in pH 2.0 buffer solution.

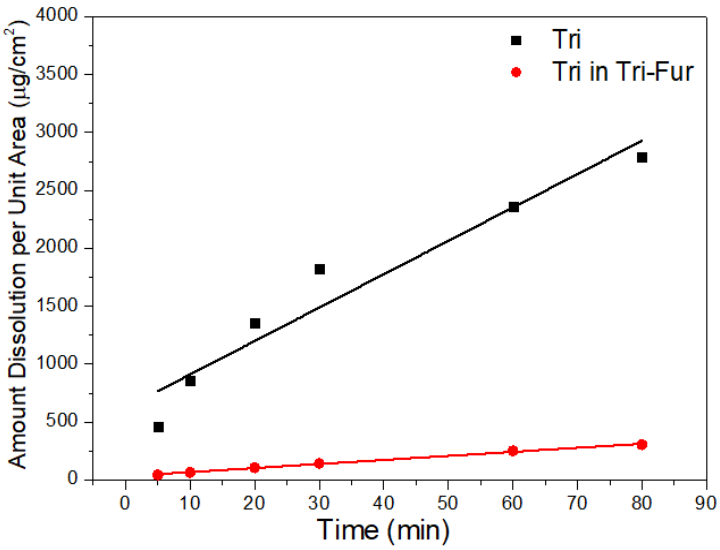

Figure S13 Intrinsic dissolution profiles of **Tri** and **Tri-Fur** in pH 2.0 buffer solution.

As shown in Fig. S12, the solubility of **Tri** in **Tri-Fur** is lower than pure **Tri** with 2.5-fold reduction. Besides, Fig. S13 shows that the IDR of **Tri** in **Tri-Fur** is lower than pure **Tri** with 8.2-fold reduction. These phenomena are mainly due to the solubility and IDR of **Tri** in **Tri-Fur** influenced by **Fur** to some extent. As the solubility of **Fur** at pH 2.0 buffer solution is low, it may form an insoluble layer to limit the **Tri** dissolution.